Materials Research Proceedings **25** (2023) 289-296 https://doi.org/10.21741/9781644902417-36

Numerical and experimental investigation on the applicability of elastomer tooling components for the manufacturing of undercut geometries by sheet metal forming

Michael Ott[1, a *], Yiran Li[1,b], Julian Krasselt[1,c], Florian Steinlehner[1,d], Patrick Haberkern[2,e], Albert Albers[2,f] and Wolfram Volk[1,g]

[1]Chair of Metal Forming and Casting, Technical University of Munich, Walther-Meissner-Strasse 4, 85748 Garching, Germany

[2]Institute of Product Engineering, Karlsruhe Institute of Technology, Kaiserstrasse 10, 76131 Karlsruhe, Germany

[a]michael.ott@utg.de, [b]yiran.li@tum.de, [c]julian.krasselt@tum.de, [d]florian.steinlehner@utg.de, [e]patrick.haberkern@kit.edu, [f]sekretariat@ipek.kit.edu, [g]wolfram.volk@utg.de

Keywords: Rapid Prototyping, Polymer, Metal Forming

Abstract. Due to their approximately hyperelastic properties, elastomers are suitable as a material for forming tools with extended forming capabilities. In this work, the use of two elastomer punches for manufacturing undercuts in sheet metal forming is performed experimentally for a demonstrator component. Since the manufacturing process does not require the use of cam slide units, it is aimed at rapid prototyping and small batch applications with the goal of reducing tooling cost and complexity. Additionally, the prediction accuracy of the elastomer tool deformation during forming was investigated in a finite element model of the manufacturing process. For comparison with the experimental implementation, punch force measurements and in-process optical strain measurements with a stereo camera system were carried out.

Introduction

The manufacturing of components with undercuts by sheet metal forming leads to challenges during the development of the tool concept. Forming operations that do not coincide with the direction of movement of the press ram are required. To perform such operations in industrial applications, cam slide units are used to deflect the direction of movement [1]. To enable the removability of the workpiece from the rigid tool after the forming step, they are commonly equipped with return springs [2]. As a design principle to keep costs and complexity low, the use of a minimum number of cam slide units for progressive forming and cutting operations is aimed at [2]. As an alternative approach to further reduce the number of cam slide units required, the formation of an undercut by reversible deformation of a punch made of an elastomer material is analysed. To prove the functionality of this approach, forming of an undercut without cam slide units is numerically evaluated and experimentally shown on a demonstrator component. This procedure is particularly aimed at prototypes, small batches and multiple variant designs.

State of the art

Current applications of elastomer tools in sheet metal forming. As alternatives to deep drawing with a rigid punch and a rigid die, DIN 8584-3 classifies deep drawing with a flexible punch and deep drawing with a flexible pad [3]. Known advantages of both approaches compared to tools made of steel are a cost-efficient and fast production of the tool components, a lower effort for the tool machining as well as a high achievable surface quality with no tool marks [4]. The disadvantages are an increased force requirement due to the additional deformation of the elastomer as well as the higher wear of the elastomer components [4]. Due to these properties, combinations of elastomer and rigid components are already widespread in industrial applications

Materials Research Proceedings **25** (2023) 289-296 https://doi.org/10.21741/9781644902417-36

for the production of small batches. Elastomer materials commonly used for this purpose are often polyurethane-based due to their chemical resistance to the lubricants used in forming as well as their mechanical wear resistance, e.g. by [5]. For the Shore A hardness, values in the range 50 to 90 are common, e.g. by [5], [6] and [7]. The high achievable elastic elongation of polymer materials can be used to realize extended shaping possibilities. For example by [8], the design of two tool concepts is shown in which an elastomer punch is used to bulge a tubular part geometry. Another recent field of research is the development of elastomer forming tool components for the production of bipolar plates [9, 10].

Numerical simulation of elastomers under mechanical load. In order to be able to predict the material flow of the elastomer components during the development of the tools, the achievable accuracy of the numerical process simulation models is essential. Hyperelastic material models based on a strain energy density function are usually applied to model the material behaviour of elastomers. Examples of approaches implemented in widely used numerical simulation programs are the models according to Mooney-Rivlin [11], Valanis-Landel [12], Ogden [13] and Arruda–Boyce [14]. Furthermore, detailed modelling approaches for the friction in the contact between elastomer tool and sheet metal have been developed in [15] and [16]. For the comparison between numerical process simulation and real process, the distribution of the strains in the manufactured sheet metal components can be carried out by an optical deformation analysis [17].

Approach

A transfer of the principle used in tube bulging [8] to sheet metal forming for the locally defined formation of undercut features in the manufactured part is investigated. The approach is implemented experimentally for a demonstrator geometry. For this purpose, a symmetric undercut is formed in a pre-bent hat-shaped profile. With rigid tools, numerical models for the design of forming processes have already reached a high degree of maturity. In order to similarly test the usability for the design of the presented manufacturing of undercuts with elastic tools, a numerical model of the manufacturing process was created using the finite element method. The comparison of simulation and experimental implementation is performed by an optical stereo measurement of one side of the punch surface during the forming of the undercut. Complementary to [17], it is not the plastic strains in the finished sheet metal component that are observed here, but the elastic strains in the elastomer punch during the process.

Structure of the forming tool. To implement the forming of the demonstrator geometry, the tool concept shown in Fig. 1 was designed and manufactured. This forming tool was integrated into a tensile-compression testing machine, AllRound Line Z 150 Zwick Roell, Ulm, Germany, with a maximum force of 150 kN. As a semi-finished product, a hat-shaped profile ① is placed in the active element of the die ②. Subsequently the elastomer punch ③ is inserted. By screwing the blank holder ④ to the die cavity ⑤, a restraining force can be applied to the flange of the sheet during subsequent forming. The vertical downward movement of the upper steel punch component ⑥ results in a compressive load on the elastomer punch. A constant value of 5 mm/min was set as the speed of the upper steel punch in the experiments. The design of the manufacturing process is based on the fact that the Poisson's ratio of the applied elastomer material has a value close to 0.5. Thus the volume of the elastomer remains approximately constant under compressive load. Therefore, compression leads to lateral deflection of the elastomer, which results in the formation of an undercut in the vertical section of the hat-shaped profile. The springback of the elastomer to the initial configuration occurring during the subsequent upward movement of the punch enables the removal of the component. The open front side can optionally be closed with a transparent pane ⑦, which ensures that observability of the process is maintained.

Materials Research Proceedings **25** (2023) 289-296 https://doi.org/10.21741/9781644902417-36

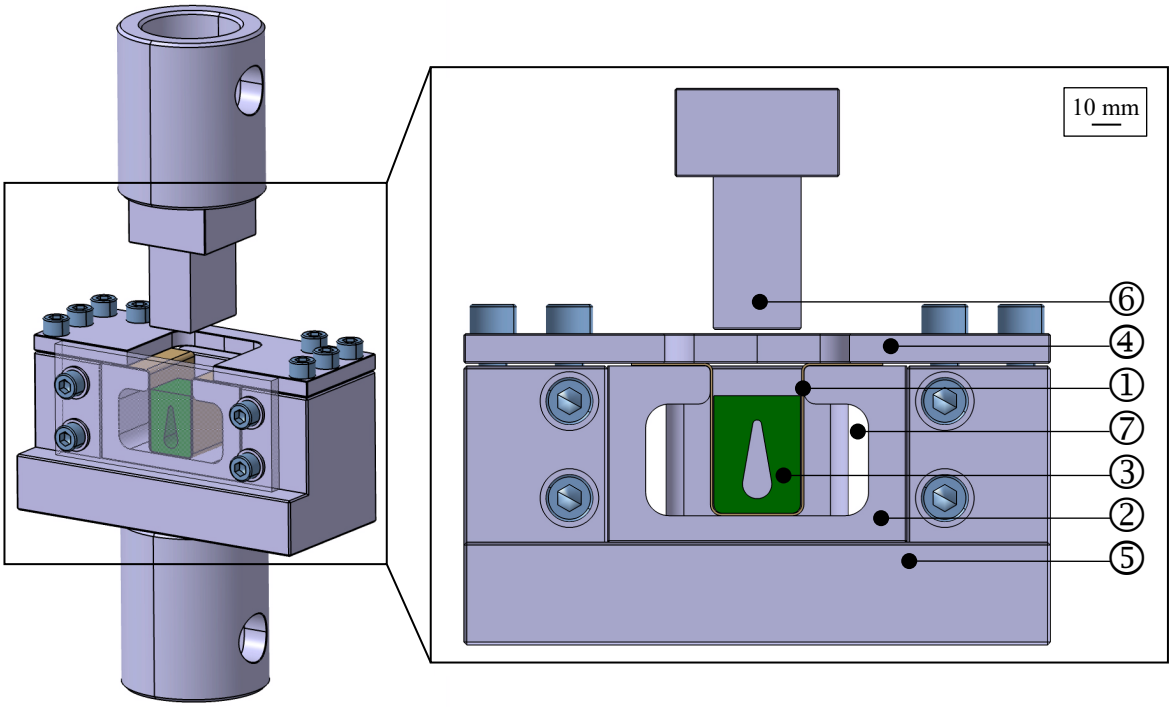

Fig. 1: Forming tool for forming of hat-shaped undercuts.

Preparation of the hat-shaped profile and the elastomer punch. The semi-finished geometry of the hat-shaped profile was bent on a Blech-Tec, Sauerlach, Germany, BT500 machine. DX56+Z100 with a sheet thickness of 0.8 mm and a non-grain oriented electrical steel sheet with a sheet thickness of 0.27 mm were used to test the suitability of the forming process for different materials and sheet thicknesses. Two different approaches were chosen for the creation of the elastomer punches. In the first approach, polyurethane with a Shore A hardness of 90 is cured through polyaddition of liquid two-component precursors. These are mixed and filled into a two-part mold of the punch. The mold was previously manufactured using the fused deposition modeling (FDM) process from polylactide (PLA) material. To reduce air inclusions in the elastomer, the polyurethane rubber is placed in a vacuum desiccator before curing and evacuated to 0.4 bar. In the second approach, additive manufacturing of the punch consisting of a rubber-like resin was carried out by photopolymer-based stereolithography (SLA) on an Anycubic Photon Mono X. Cleaning with isopropanol and subsequent curing with UV light were necessary as final manufacturing steps for the component generated by this method. As shown in Fig. 2, this punch contains a central opening to demonstrate the expanded shape capabilities of the direct additive manufacturing approach. Partial support structures, which could easily be removed manually afterwards, were required for creating the opening.

Materials Research Proceedings **25** (2023) 289-296 https://doi.org/10.21741/9781644902417-36

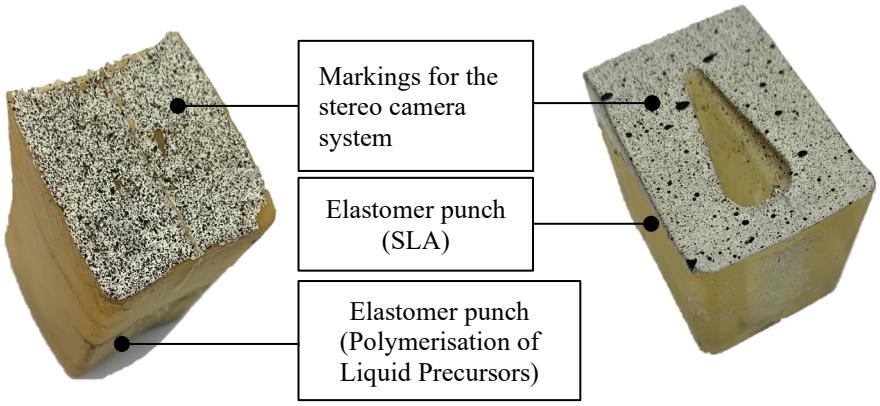

Fig. 2: Elastomer punches after preparation for the stereo camera measurements.

Sensor technology for comparison with the simulation model. The force acting on the steel punch and the displacements in the elastomer punch component are defined as criteria for evaluating the prediction accuracy of the simulation model. For comparison with the physical process, a load cell in the testing machine is used to determine the punch force versus the vertical punch position. A stereo camera system can be used to record the displacements during forming on the openly accessible front side of the elastomer. The GOM Aramis SRX system was used for this purpose with a frame rate of 1 Hz. For the preparation of the elastomers, a white colour base layer and a black stochastic dot pattern are coated on the front side of the punch, as shown in Fig. 2. From the acquired images, the strains in the marked area are calculated using Digital Image Correlation (DIC).

Structure of the simulation model. A numerical model of the manufacturing process was created in LS-DYNA using a Lagrangian finite element formulation as shown in Fig. 3. Following an explicit forming step, an implicit step was performed to calculate the springback of the sheet. Both the DX56 sheet and the electrical sheet were discretized by shell elements. For the modelling of the plastic material behaviour with the Hill48 model, data from previous tensile tests were available. For the non-linear stress-strain relation of the two elastomers, the hyperelastic material model according to Mooney-Rivlin (MAT_027 [18] in LS-DYNA) was used. The vertical punch movement during forming results predominantly in compressive stresses in the elastomer punch. Thus, for parameterization of the material model compression tests were carried out with the two materials on a Zwick Roell tensile-compression testing machine. Cylindrical specimens, produced under the same manufacturing conditions as the two elastomer punches, were used for this purpose. The resulting parameter values for MAT_027 are shown in Tab. 1, including the two empirically determined material constants of the Mooney-Rivlin model referred to as A and B.

Tab. 1: Shore A hardness and parameter values for the hyperelastic material model.

	Shore A hardness	**Mass density [g/cm^3]**	**Poisson's ratio**	**Constant A**	**Constant B**
SLA material	95	1.1	0.495	4.82	-0.59
Polyurethane	90	1.0	0.495	4.63	-0.72

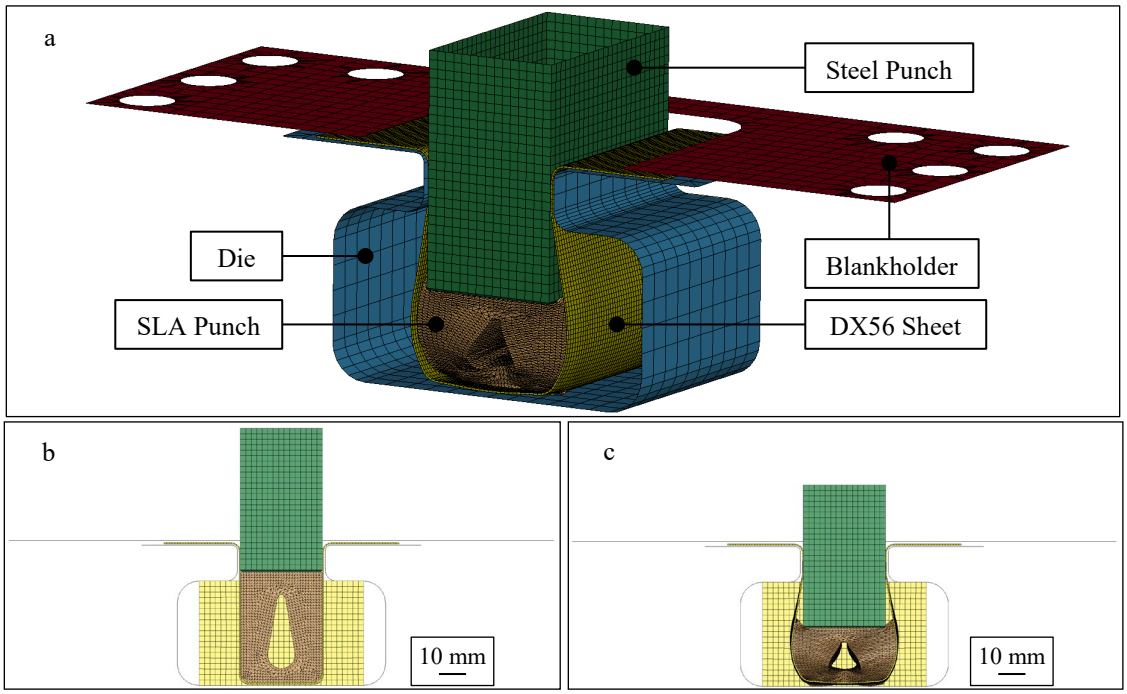

Fig. 3: Numerical simulation model of the forming process: Isometric view (a), front view with punch in top dead centre (b) and bottom dead centre position (c).

Results

Manufacturing of the demonstrator geometry with undercut. For both sheet materials investigated, the formation of a symmetrical undercut in the vertical section of the top hat profile was achieved with both of the punches. The resulting final part geometry after springback is shown in Fig. 4 for the DX56+Z100 sheet. A maximum overlap of 7 mm with the DX56 and 11 mm per side with the electrical sheet were achieved for the formed symmetrical undercut geometry. Compared to the initial width of the vertical sheet section of 30 mm, this corresponds to an increase in width of 47 % for the DX56 specimen and 73 % for the electrical sheet. In the bottom dead centre position, both punches were compressed by 20 mm. For the SLA-generated punch, this resulted in a maximum principal strain of 43.6 % measured by the stereo camera system. For the springback during the load release phase, both elastomers exhibit a viscoelastic behaviour. As shown in the image taken by one of the stereo cameras in Fig. 5, the elastomer punch does not follow the upward steel punch movement instantaneously. Instead it takes approximately 60 s for both punches to return to the initial geometry. To assess the durability of the tools, ten process repetitions were carried out. Neither significant wear on the two punches nor negative effects on the repeatability of the final sheet geometry were observed.

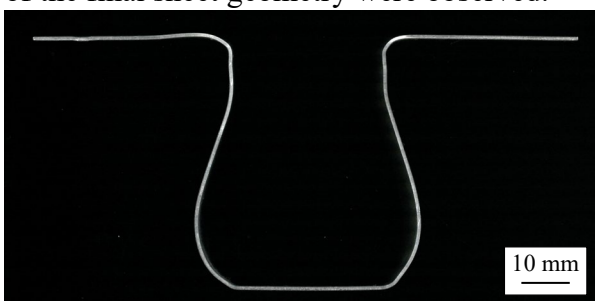

Fig. 4: Cross section of the resulting demonstrator geometry after springback (DX56+Z100).

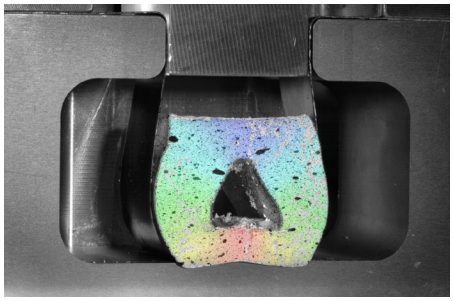

Fig. 5: Stereo camera image taken during the load release phase.

Comparison of the simulation model with the experimental implementation. Delamination of the colour coating occurred during forming at higher deformations for the punch produced by

Materials Research Proceedings **25** (2023) 289-296 https://doi.org/10.21741/9781644902417-36

polymerisation of liquid precursors. Therefore, the comparison of simulation and measurements is performed for the SLA punch. For this configuration, the numerical model calculated stably up to reaching the lowest punch position examined in the experiment at a vertical displacement of -20 mm. As the first comparison criterion, the measured horizontal and vertical displacements in bottom dead centre position are shown in comparison to the simulation model in Fig. 6. An indication of the accuracy of the stereo camera measurements is the symmetry of the results. The numerical model shows the horizontal bulging of the elastomer. In addition, the formation of the upper two corners of the punch is predicted.

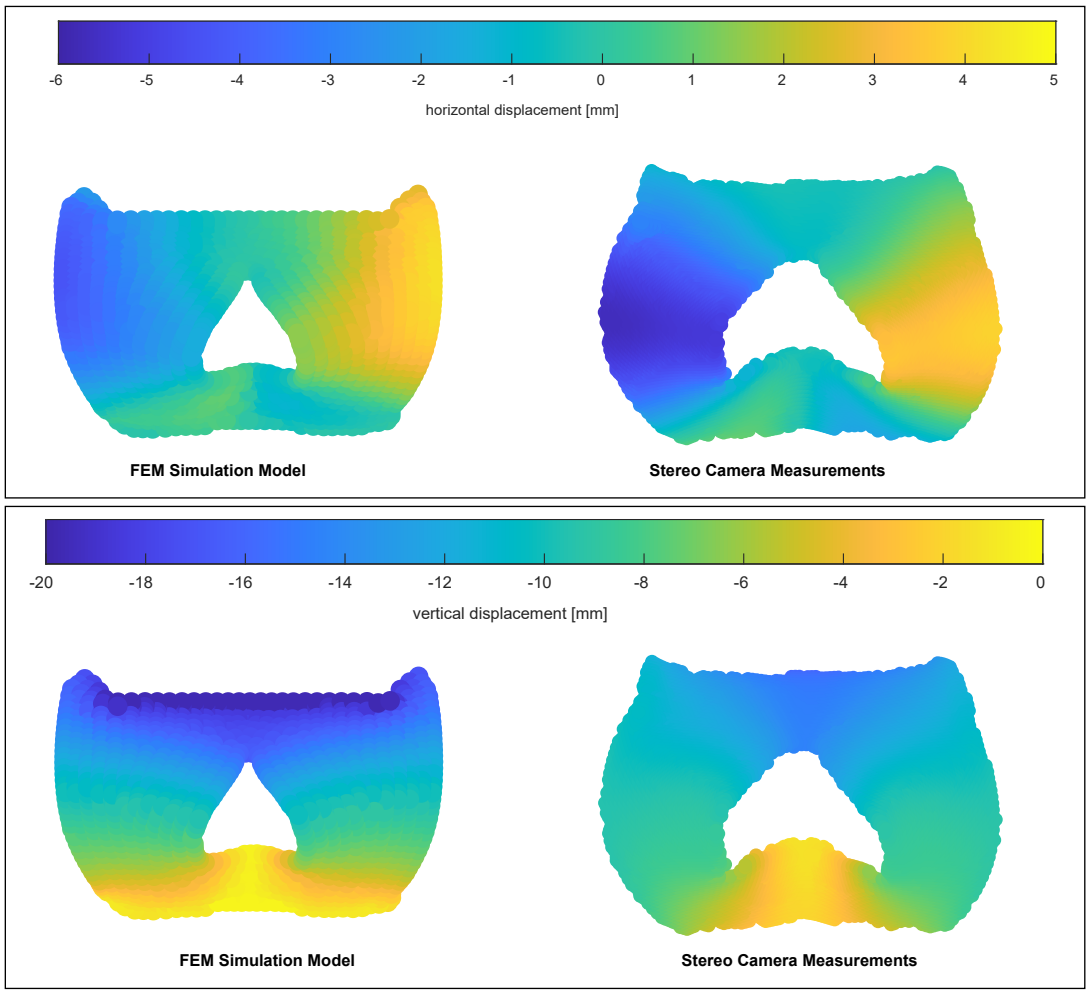

Fig. 6: Displacements (horizontal and vertical component) on the elastomer front side: calculation in the FEM simulation model and in-process measurements in the bottom dead centre position for the SLA-manufactured punch.

As the second comparison criterion, calculated and measured punch force - displacement curves are shown in Fig. 7. The initial height of the SLA punch was 40 mm. Up to a displacement of 10 mm, a good prediction accuracy of the simulation model is obtained. For larger deformations, the deviations increase. Further mesh refinement as a possible measure to increase the accuracy at high strains leads to a significant increase in the calculation time for the comparatively small elastomer punch. This would contradict the planned application goal of tool development for rapid prototyping applications. The main proportion of the force results from the deformation of the elastomer and only minor differences were measured when the experiment was performed without an inserted plate.

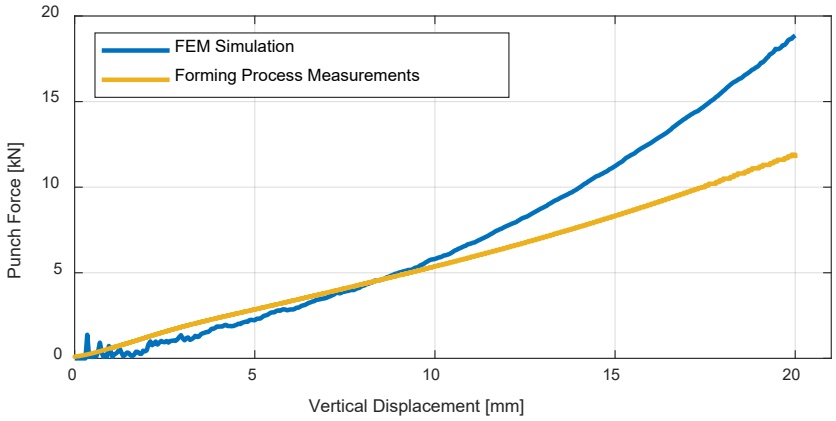

Fig. 7: Punch force - displacement curves: calculation in the FEM simulation model and measurement in the forming process.

Summary and Outlook

The experimental results obtained on the demonstrator geometry show the practical applicability of mechanical compression of an elastomer punch for local forming of undercuts. Overlaps up to 11 mm per side were achieved. Due to the almost complete springback of the punches to the initial configuration, removal of the parts from the forming tool set was made possible. The viscoelastic behaviour of the elastomer materials and the resulting time required for springback had a limiting effect on the achievable process times. However, this aspect often plays only a subordinate role for the intended application area of small batch production. Furthermore, the combination with the pre-bent hat-shaped profiles demonstrates the integration capability of the elastomer tools in multi-stage forming processes. Thus, the possibilities for prototyping can be expanded as in the manufacturing sequence shown in combination with swivel bending. Both the polymerisation of liquid precursor components in an additive manufactured mold and the direct additive manufacturing by the SLA process proved suitable for the production of elastomer tool components. Potentials of the second approach are an increased freedom of shape of the tool components and a further reduction of tool development times by eliminating the mold manufacturing.

The corresponding numerical process model shows stable behaviour despite the high strains in the elastomer during forming. Therefore it can be considered as an appropriate tool for simulative design and validation during the tool development. Both for the forces on the upper rigid punch component and for the in-process displacement measurements on the elastomer punch, there is good correlation up to punch displacements of 10 mm. For higher strains, the differences increased, especially for the predicted punch force. To further improve the agreement of the simulation and the experiment, more accurate models of the tribology between elastomer and sheet can be investigated. Space-fixed Eulerian meshing or the Element-Free Galerkin method can also be examined for applications with such high deformations of the elastomer in future work.

Acknowledgements

The authors gratefully acknowledge the German Research Foundation (Deutsche Forschungsgemeinschaft, DFG) for supporting this work carried out within the framework of the collaborative research project 431606085 (VO 1487/51-1).

References

[1] R. Canti, Analyse für eine belastungsgerechte Auslegung von Presswerkzeugen am Beispiel Niederhalter und Schiebersystem, PhD thesis, Technische Universität München, 2016.

[2] A. Birkert, S. Haage, M. Straub, Umformtechnische Herstellung komplexer Karosserieteile, Springer Berlin Heidelberg, Berlin, Heidelberg, 2013. https://doi.org/10.1007/978-3-662-46038-2

[3] DIN Deutsches Institut für Normung e.V., DIN 8584-3:2003-09, 2003.

[4] M. Ramezani, Z.M. Ripin, Rubber-pad forming processes: Technology and applications, Woodhead Publishing, 2012. https://doi.org/10.1533/9780857095497

[5] Y. Liu, L. Hua, J. Lan, X. Wei, Studies of the deformation styles of the rubber-pad forming process used for manufacturing metallic bipolar plates, J. Power Sources, 195 (2010) 8177–84. https://doi.org/10.1016/j.jpowsour.2010.06.078

[6] A. del Prete, G. Papadia, B. Manisi, Computer Aided Modelling of Rubber Pad Forming Process, KEM 473 (2011) 637–44. https://doi.org/10.4028/www.scientific.net/KEM.473.637

[7] L. Belhassen, L. Ben Said, S. Koubaa, M. Wali, Effects of Using Flexible Die Instead of Flexible Punch in Rubber Pad Forming Processm, in: M. Haddar, F. Chaari, A. Benamara, M. Chouchane, C. Karra, N. Aifaoui, (Eds.), Design and Modeling of Mechanical Systems-III, Springer International Publishing, Cham, 2018, pp. 259–267. https://doi.org/10.1007/978-3-319-66697-6_26

[8] Fibro GmbH, Hauptkatalog Update 2022, available on https://www.fibro.de/fileadmin/FIBRO/Blaetterkataloge/Hauptkatalog_DE/HTML5/1194/index.html, accessed 9 January 2023.

[9] Y. Liu, L. Hua, Fabrication of metallic bipolar plate for proton exchange membrane fuel cells by rubber pad forming, J. Power Sources 195 (2010) 3529–35. https://doi.org/10.1016/j.jpowsour.2009.12.046

[10] M. Elyasi, F.A. Khatir, M. Hosseinzadeh Manufacturing metallic bipolar plate fuel cells through rubber pad forming process, Int J Adv Manuf Technol 89 (2017) 3257–69. https://doi.org/10.1007/s00170-016-9297-6

[11] R.S. Rivlin, Large elastic deformations of isotropic materials IV. Further developments of the general theory, Phil. Trans. R. Soc. Lond. A 241 (1948) 379–97. https://doi.org/10.1098/rsta.1948.0024

[12] K.C. Valanis, R.F. Landel, The Strain-Energy Function of a Hyperelastic Material in Terms of the Extension Ratios, J. Appl. Phys. 38 (1967) 2997–3002. https://doi.org/10.1063/1.1710039

[13] R.W. Ogden, Large deformation isotropic elasticity – on the correlation of theory and experiment for incompressible rubberlike solids, Proc. R. Soc. Lond. A 326 (1972) 565–84. https://doi.org/10.1098/rspa.1972.0026

[14] E.M. Arruda, M.C. Boyce, A three-dimensional constitutive model for the large stretch behavior of rubber elastic materials, J. Mech. Phys. Solids, 41 (1993) 389–412. https://doi.org/10.1016/0022-5096(93)90013-6

[15] L. Deladi, Static friction in rubber-metal contacts with application to rubber pad forming processes, PhD thesis, University of Twente, 2006.

[16] M. Ramezani, Z.M. Ripin, R. Ahmad, Computer aided modelling of friction in rubber-pad forming process, J. Mater. Process. Technol. 209 (2009) 4925–34. https://doi.org/10.1016/j.jmatprotec.2009.01.015

[17] S. Kut, B. Niedziałek, Numerical And Experimental Analysis Of The Process Of Aviation Drawpiece Forming Using Rigid And Rubber Punch With Various Properties, Arch. Metall. Mater. 60 (2015) 1923–8. https://doi.org/10.1515/amm-2015-0327

[18] Livermore Software Technology, LS-DYNA Keyword User's Manual - Volume II Material Models (R13), available on https://www.dynasupport.com/manuals/ls-dyna-manuals, accessed 9 January 2023.